PERFORMANCE REPORT SUBMITTED TO:

National Aeronautics and Space Administration (NASA)
Lewis Research Center
Attn: Mr. Kenneth A. DeLaat
21000 Brookpark Road
Mail Stop 500-315
Cleveland, OH 44135

COOPERATIVE AGREEMENT TITLE:

"Development of Collaborative Research Initiatives to Advance the Aerospace Sciences - Emphasis in Power Electronics"

COOPERATIVE AGREEMENT NUMBER:

NCC3-324

PERFORMANCE REPORT:

September 15, 1993 through September 14, 1994

SUBMITTED BY:

T. Michael Knasel
Director for Research
Ohio Aerospace Institute
22800 Cedar Point Road
Cleveland, OH 44142
216/962-3040

January 9, 1995

Contents

List of Figures

PREFACE

This report was prepared for NASA LeRC.

Acknowledgments

Many thanks to NASA LeRC and Wright Laboratory for their support of this project. The research accomplished was primarily completed by The Ohio State University.

1. The DSP56001 Development System

1.1 Introduction

Single-chip microprocessors are widely used in the motion control industry. The single-chip implementation is economic and compact, but inflexible. This inflexibility restricts an engineer when quick laboratory implementation and testing of a new control scheme are desired. The need for a quick and flexible means to test new control methods has prompted the design of a general purpose DSP 56001 development system. With this system, new control algorithms can be quickly tested and evaluated. If satisfactory system performance is achieved, then a dedicated single-chip controller can be constructed. This methodology shortens the development time while increasing system reliability.

At present, most DSP based implementation of motion control is based on the products of the TMS family [1]. In this paper, a general purpose, flexible Motorola DSP56001 development system (DSP56KDS) for motion control is presented. The core processor is a DSP56001 and uses a non-obstructive three-stage instruction fetch/decode/execute pipeline combined with three independent execution units. These three independent units are the data ALU, the address generation unit, and the program controller. These units are connected by four 24-bit data buses and three 16-bit address buses to three independent on-chip memory blocks, providing the parallelism needed for high performance signal processing. This parallelism allows, for example, 13.5 million instructions to be executed in only one second at a clock rate of 27 MHz. The DSP56001 has three multimode on-chip peripherals which enchance its performance and contribute to a compact system layout. In addition, a reduction in overall cost occurs. The expanded memory and user peripheral boards can be conveinently connected to the DSP56001 through these three multimode ports.

The DSP56KDS consists of three sections: i) the DSP56001 core processor, ii) the bus interface board, and iii) several peripheral boards including a 4-channel A/D and D/A board, a sine-triangle PWM board, a multifunctional digital PWM board, an encoder board, and a digital I/O board. All these peripheral boards are configured on the VME bus and communicate with the core DSP processor through the bus interface board. A personal computer is used to write the control program in either C or assembly language. The control program is then loaded into the DSP through the pc interface board.

The configuration and operating principles of the DSP56KDSare presented in the following sections, including the hardware and software organization. A detailed discussion of peripheral board design, so critical for motion control, is included in the hardware description. The basic equations of the brushless DC (BLDC) machine follow. Finally, experimental results of a vector controlled BLDC machine with full digital implementation are given to illustrate the high performance characteristics of the DSP56KDS.

1.2 Configuration and Operation Principles

The complete DSP 56001 based motion control development system is shown in Figure 1.1. The dsp controller is connected with the bi-directional power flow converter via the base driver circuitry. The inverter then supplies voltage to the machine with the capability of reverse power flow. The personal computer is used to download control programs to the DSP 56001.

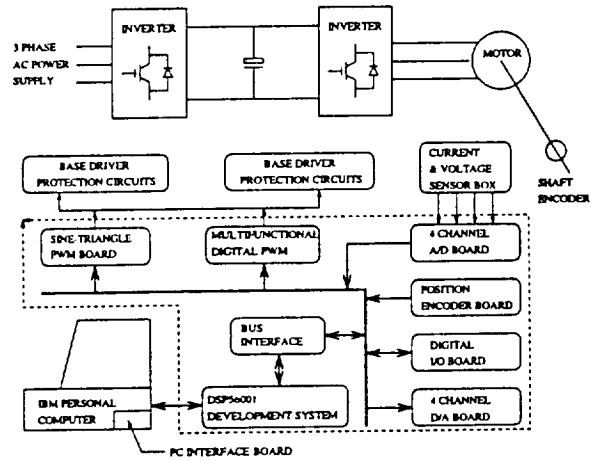

Figure 1.1: DSP56001 Motion Control Development System

1.2.1 Hardware Configuration

The hardware configuration of the DSP56KDSemphasizes integration between the core processor and peripheral boards to increase processing speed and reliability. The ability to implement many different control algorithms with the same hardware makes the DSP56KDShighly flexible.

The hardware configuration enables the core processor to easily communicate with the peripheral boards. The currents, voltages, and rotor positions are conveniently input to the core processor through the 4-channel A/D and encoder board. Control signals are then synthesized within the DSP, and are output to the inverter throught the sine-triangle or multifunctional digital PWM board. All of the input and output signals to the DSP are sent through parallel ports, making the controller very fast.

The multifunctional digital PWM board consists of four 12-bit up-down counters and logic circuits. The output states of the PWM can be preset and cleared. The time constants calculated by software are sent to these counters. When time is out, the output states of the PWM are toggled. This method allows for different PWM algorithms to be executed with the same hardware. Different PWM schemes of interest are hysteresis band, space vector, etc. The ability to implement various PWM algorithms and change the control laws with the same hardware configuration gives

the DSP56KDSthe capability to control many different types of machines such as the induction, switched reluctance, and BLDC.

The encoder board is designed to function as both an incremental and absolute encoder. This is done by using the index pulse to clear the counter so that an absolute position is obtained by adding an initial index offset. Typical encoder waveforms are shown in Figure 1.2. The comm-r,s,t waveforms give the position of the rotor poles via the Hall communication sensors, and the motor-r,s,t waveforms are the command currents.

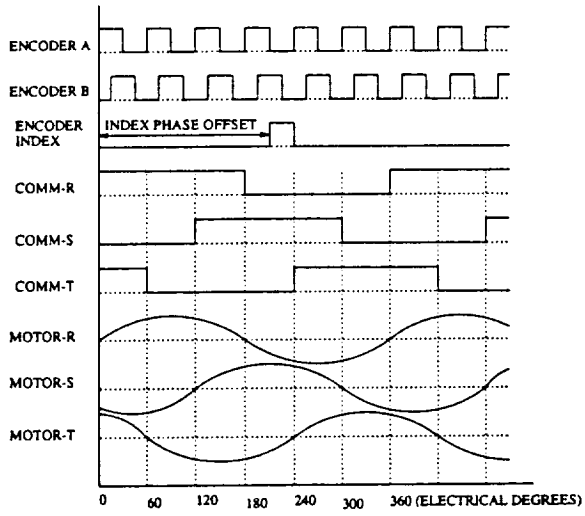

Figure 1.2: Encoder Waveforms

The hardware components of the DSP56KDSinclude the A/D and D/A converters, incremental/absolute encoder, multifunctional and sine-triangle PWM boards, and digital I/O board. A bus interface board connects these components to the core processor to form a highly integrated and flexible motion control system.

1.2.2 Software Organization

The software in the DSP can be configured to implement sophisticated algorithms for torque, speed, and position control. The type of electric machine selected can vary, with the necessary adjustments for the control system being made in the software.

The software of the DSP56KDS is organized into modular forms. Modular sections for current, speed, and position control are optimized to reduce storage effects and shorten execution time. Another modular section developed is reference frame transformation for vector or field oriented control. These basic sections can be combined together to form a complicated program, capable of sophisticated motion control. Examples of sophisticated control include field oriented control of induction machines, position sensorless control of doubly excited variable speed contant frequency generators, and variable speed switched reluctance machines [2-4].

The modular software organization of the DSP56KDSallows for flexible implementation of high performance motion control algorithms. The modular structure reduces development time, speeding the overall design process.

1.2.3 Basic Equations of the Brushless DC Machine

The voltage and torque equations of the BLDC machine in the rotor reference-frame are expressed as follows:

$$v_{qs} = (r_s + pL_q)i_{qs} + \omega_r L_d i_{ds} + \omega_r \lambda_m \quad (1.1)$$

$$v_{ds} = (r_s + pL_q)i_{ds} - \omega_r L_q i_{qs} \quad (1.2)$$

$$T_e = \frac{3}{2}\frac{p}{2}[\lambda_m i_{qs} + (L_d - L_q)i_{qs}i_{ds}] \quad (1.3)$$

Where i_{ds}, i_{qs} are the d and q axis components of armature current, v_{ds}, v_{qs} are the d and q axis components of terminal voltage, and λ_m is the rotor flux.

The state of the communication Hall sensor or encoder provides the information regarding the position of the poles, and thus the position of the q and d axes. When the machine is placed in field orienation, the q and d axis currents are decoupled. The current i_{ds} is held constant, and the torque is independently controlled by modulating i_{qs}.

1.3 Experimental Results

The example chosen to illustrate the advantages of the DSP56KDSis a servo system based on the BLDC machine. The BLDC machine is quite suited for high precision servo applications, such as machine tools, robotics, and computer peripherals.

Position and speed tracking are precisely controlled with the BLDC machine to create a high performance motion control system. The control system block diagram is shown in Figure 1.3, while the control algorithm flowchart is shown in Figure 1.4.

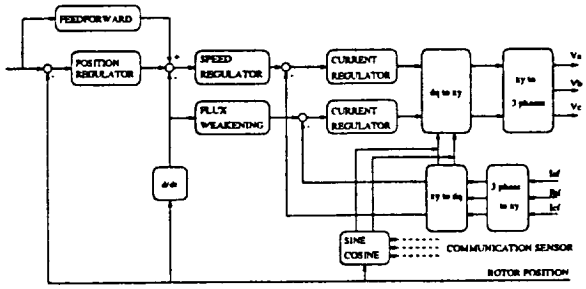

Figure 1.3: BLDC Control System Block Diagram

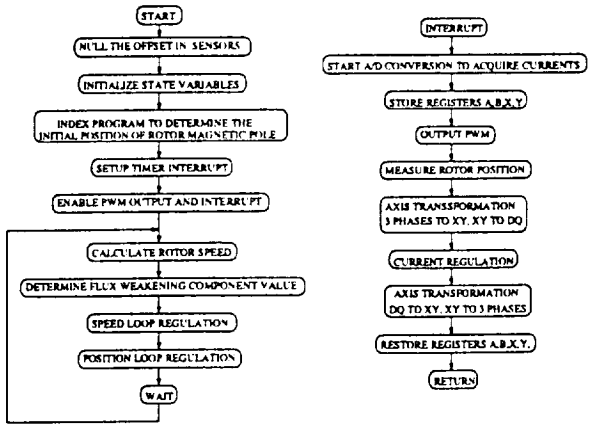

Figure 1.4: Control Algorithm Flowchart

Three control loops are implemented: torque, speed, and position. The inner most loop controls the current for instantaneous torque response, updating the torque command every 50 μsec. The second loop is for speed regulation where the speed command is updated every 250 μsec. The outer loop is for position control. The experimental results of the servo system are shown in Figure 1.5, Figure 1.6, and Figure 1.7.

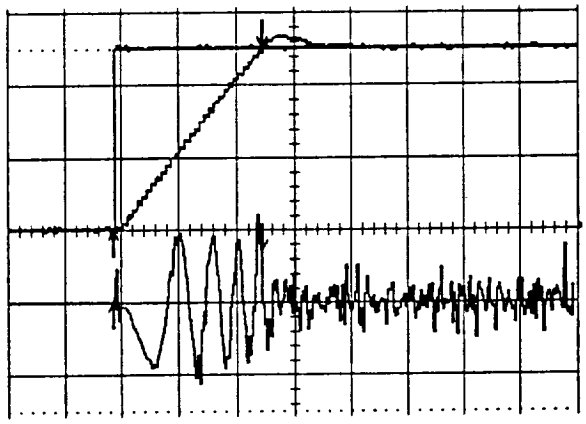

Figure 1.5: Current and Speed Regulation

Figure 5 shows the experimental results of current and speed regulation in response to a step command in speed. The top portion of the figure is the speed command and actual rotor speed, and the bottom part is the phase current. Noting that the time base is 10 ms/div, the rotor accelerates from zero to 4500 rpm within 25 msec. There is a small amount of overshoot, but the speed is quickly clamped to 4500 rpm at approximately 32 msec. The rapid speed response is created by the field oriented controller, which enables maximum torque capability even in transient conditions.

Figure 6 shows four quadrant operation of the BLDC machine within a speed range

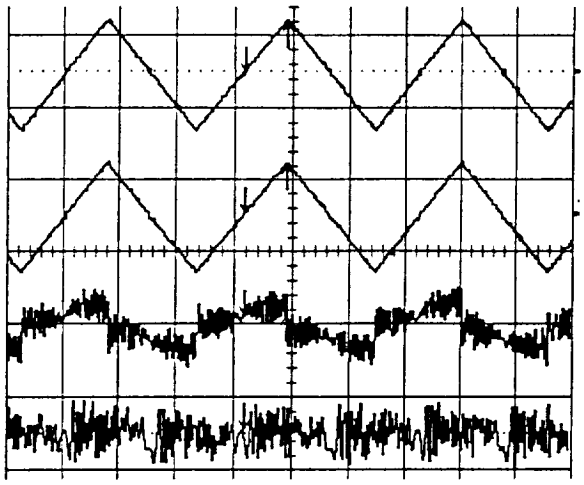

Figure 1.6: Four Quadrant Operation

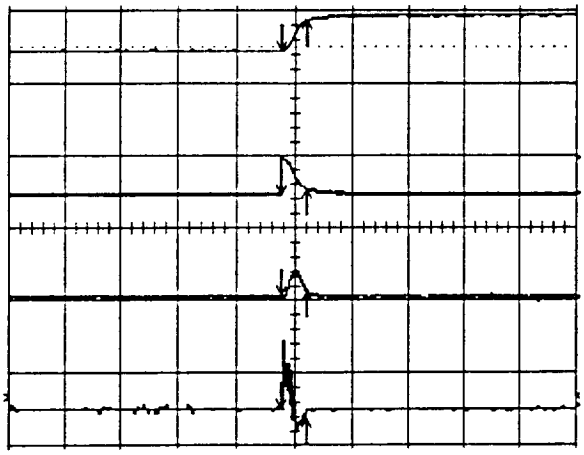

Figure 1.7: Responses to Rotor Position Step Command

of +/- 3600 rpm. Shown in the figure are the command speed, actual speed, torque current I_{qs}, and phase current. The transient torque current is precisely controlled, enabling the rotor speed to exactly follow the command speed. The current has zero frequency at zero speed, a result of field oriented control.

Figure 7 shows responses to a rotor position step command of 90 electrical degrees. The top waveform in the figure is the rotor position. The second waveform is the rotor position error. The rotor speed and torque current are the bottom two waveforms. Initially, the rotor position error is large when the step command is given. However, the rotor position error rapidly decreases to zero. The rotor speed, the third waveform in the figure, increases for a short period and then decreases to zero as the position error approaches zero. The torque current, I_{qs}, increases and then decreases in accordance with the rotor speed.

The experimental results obtained demonstrate the high performance control achieved by the DSP56KDS. Speed tracking is successfully implemented for a step command and four quadrant operation, while the rotor position is accurately controlled for a step command of 90 electrical degrees.

1.4 Chapter Summary

A general purpose, flexible DSP development system using the Motorola DSP56001 is developed for motion control. The overall system configuration is presented, including the hardware and software organization. Peripheral board design is included as part of the hardware discussion, and the modular software structure for controlling different types of machines is discussed. A field oriented BLDC servo system is implemented to demonstrate the numerous advantages of the DSP56KDS.

2. Position Sensorless Induction Machine Drive

2.1 Introduction

High performance electrical drives are being considered in the aerospace industry to replace hydraulic actuators, improve older electrical actuation systems, and as starter /generator systems for gas turbines [14]. The recent progress in power electronics has made variable frequency drive systems quite attractive for aerospace applications, with the reluctance machine receiving much attention [15]. The cage rotor or doubly fed induction machine still has several noteworthy advantages, however, including field weakening, tough and rugged construction, low cost, and simplified inverter/machine interface. The *sensorless* operation of an induction machine is attractive for aerospace applications because of increased reliability, decreased overall cost, and a less restrictive geometry for the drive.

Many sensorless drives have been developed using different approaches. A physical approach was taken in [7], while more control oriented approaches were taken in [8, 9]. In [7], the authors presented a rotor flux oriented, position sensorless induction machine drive and showed that if the normal integration process is used to calculate the rotor flux, changing parameter values and low speed effects will result in an incorrect estimate. An inaccurate rotor flux estimate, in turn, produces an incorrect rotor speed estimate. The authors of [7] proposed a solution in which simple low pass filtering of both the back emf and flux command is done, resulting in a robust flux estimator which is largely insensitive to parameter variations and works well in a low speed range. In [8], the authors used the difference between two flux estimators and proposed a novel pole assingment method to realize a robust flux observer. This approach is more of a control oriented approach because of the use of Popov's criteria, linearization, and state-space pole assignment. There is less emphasis on machine physics, and how the machine physics affect rotor flux estimation. In [9], adaptive control theory is applied to synthesize an estimator. In addition, the estimator uses a parameter adaptive scheme to compensate for changing parameter values. For these reasons, we classify the approach in [9] as control oriented as well.

Two principle advantages exist in developing a drive using the approach of [7]. One, there is essentially no control system design needed to produce the flux estimator. No time is required to tune the estimator. For the physical approach, the critical information needed for implementation is the value of the rotor time constant. Two, the estimation algorithm is easily implemented in a DSP or dedicated hardware.

Rotor field orientation is reviewed, and the system structure for the rotor flux estimator is presented. The speed estimator scheme is discussed. The accuracy is of the estimator is first tested on a indirect field oriented drive, and then a closed loop direct field oriented drive using the physical flux estimator is constructed. Computer simulation and laboratory results are presented to show the success of the approach.

2.2 Rotor Field Orientation

2.2.1 Machine Model

The synchronous frame, rotor flux oriented d-q induction machine model is shown in Figure 2.1.

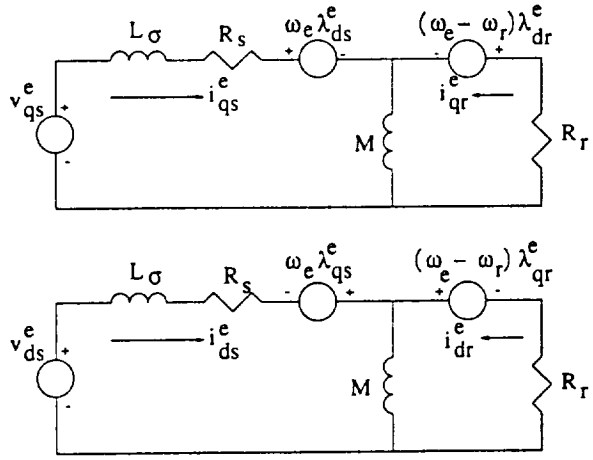

Figure 2.1: Rotor Flux d-q Model

The fifth order set of differential equations which describe a three phase symmetrical induction machine are:

$$v^e_{qs} = L_\sigma \frac{di^e_{qs}}{dt} + R_s i^e_{qs} + \omega_e \lambda^e_{ds} + \frac{d\lambda^e_{qr}}{dt} \tag{2.1}$$

$$v^e_{ds} = L_\sigma \frac{di^e_{ds}}{dt} + R_s i^e_{ds} - \omega_e \lambda^e_{qs} + \frac{d\lambda^e_{dr}}{dt} \tag{2.2}$$

$$v^e_{qr} = R_r i^e_{qr} + (\omega_e - \omega_r)\lambda^e_{dr} + \frac{d\lambda^e_{qr}}{dt} \tag{2.3}$$

$$v^e_{dr} = R_r i^e_{dr} - (\omega_e - \omega_r)\lambda^e_{qr} + \frac{d\lambda^e_{dr}}{dt} \tag{2.4}$$

$$T_e = J\frac{d\omega_{rm}}{dt} + B_m \omega_{rm} + T_l \tag{2.5}$$

where

$$\lambda^e_{qr} = M(i^e_{qs} + i^e_{qr}) \tag{2.6}$$

$$\lambda^e_{dr} = M(i^e_{ds} + i^e_{dr}) \tag{2.7}$$

$$T_e = \frac{3P}{4}(\lambda^e_{dr} i^e_{qs} - \lambda^e_{qr} i^e_{ds}) \tag{2.8}$$

The first principle of field orientation is to align the rotor flux with the d axis. This forces $\lambda^e_{qr} = 0$. The conditions for field orientation control are derived from the rotor

voltage and rotor flux equations listed above, with the condition $\lambda^e_{qr} = 0$. Equations (2.3) (2.4) (2.6) (2.7) and (2.8) are listed in reduced form:

$$(\omega_e - \omega_r) = \frac{-R_r i^e_{qr}}{\lambda^e_{dr}} \tag{2.9}$$

$$\frac{d\lambda^e_{dr}}{dt} = -R_r i^e_{dr} \tag{2.10}$$

$$i^e_{qs} = -i^e_{qr} \tag{2.11}$$

$$\lambda^e_{dr} = M(i^e_{ds} + i^e_{dr}) \tag{2.12}$$

$$T_e = \frac{3P}{4}(\lambda^e_{dr} i^e_{qs}) \tag{2.13}$$

The slip condition is found by inserting (2.11) into (2.9);

$$\omega_e - \omega_r = s\omega_e = \frac{R_r i^e_{qs}}{\lambda^e_{dr}} \tag{2.14}$$

From Equation (2.12),

$$i^e_{dr} = \frac{\lambda^e_{dr}}{M} - i^e_{ds} \tag{2.15}$$

The flux condition is found by inserting (2.15) into (2.10);

$$\lambda^e_{dr} = \frac{M i^e_{ds}}{1 + T_r p} \tag{2.16}$$

where T_r is the rotor time constant and is equal to

$$T_r = \frac{M}{R_r} \tag{2.17}$$

2.2.2 Rotor Flux Estimation Scheme

The stationary frame *vector* model of the rotor flux oriented induction machine is shown in Figure 2.2. This model is chosen because it is the basis for rotor flux estimation. The block diagram of the proposed rotor flux estimator is shown in Figure 2.3.
Note that the block diagram realizes the rotor flux estimator according to the following equation:

$$\vec{\lambda}^s_{qdr} = \frac{T_c \vec{E}^s_c}{1 + T_c p} + \frac{\vec{\lambda}^{s*}_{qdr}}{1 + T_c p} \tag{2.18}$$

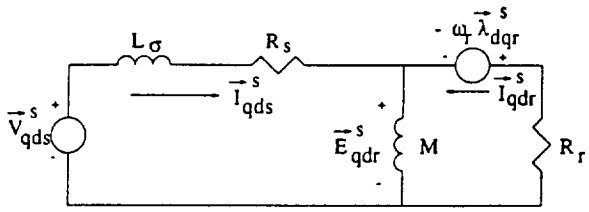

Figure 2.2: Vector Model in Stationary Frame

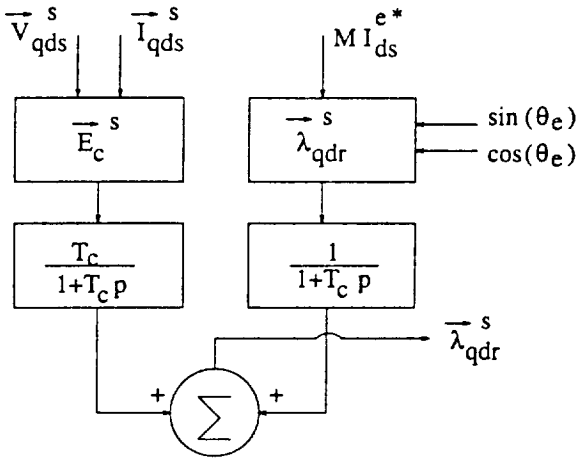

Figure 2.3: Flux Estimator Block Diagram

The frequency domain version of (2.18) is:

$$\vec{\lambda}^s_{qdr} = \frac{T_c \vec{E}^s_c}{1 + j\omega_e T_c} + \frac{\vec{\lambda}^{s*}_{qdr}}{1 + j\omega_e T_c} \tag{2.19}$$

where the vectors are defined as:

$$\vec{\lambda}^{s*}_{qdr} = \begin{bmatrix} \lambda^{s*}_{qr} \\ \lambda^{s*}_{dr} \end{bmatrix} \vec{E}^s_c = \begin{bmatrix} E^s_{cqr} \\ E^s_{cdr} \end{bmatrix} \vec{\lambda}^s_{qdr} = \begin{bmatrix} \lambda^s_{qr} \\ \lambda^s_{dr} \end{bmatrix} \tag{2.20}$$

Using the stator voltages and currents, the calculated back emf, $\vec{E}^s_c$, is given by:

$$\vec{E}^s_c = \vec{V}^s_{qds} - (R^*_s + j\omega_e L^*_\sigma)\vec{I}^s_{qds} \tag{2.21}$$

where R^*_s and L^*_σ are the nominal values of stator resistance and leakage inductance. The nominal values are related to the actual values by:

$$R^*_s = R_s - \Delta R_s \tag{2.22}$$

$$L^*_\sigma = L_\sigma - \Delta L_\sigma \tag{2.23}$$

Inserting (2.22) and (2.23) into (2.21) yields:

$$\vec{E}_c^s = \vec{V}_{qds}^s - ((R_s - \Delta R_s) + j\omega_e(L_\sigma - \Delta L_\sigma))\vec{I}_{qds}^s \tag{2.24}$$

According to Figure 2.2, the actual back emf, $\vec{E}_{qdr}^s$, is

$$\vec{E}_{qdr}^s = \vec{V}_{qds}^s - (R_s + j\omega_e L_\sigma)\vec{I}_{qds}^s \tag{2.25}$$

Therefore, the calculated and actual back emfs are related by

$$\vec{E}_c^s = \vec{E}_{qdr}^s + (\Delta R_s + j\omega_e \Delta L_\sigma)\vec{I}_{qds}^s \tag{2.26}$$

For notation purposes, the following expressions are introduced:

$$\vec{\mu} = \frac{1}{1 + j\omega_e T_c} = |\vec{\mu}| \angle\phi \tag{2.27}$$

where

$$|\vec{\mu}| = \frac{1}{\sqrt{1+(\omega_e T_c)^2}} \quad \text{and} \quad \angle\phi = -tan^{-1}(\omega_e T_c) \tag{2.28}$$

Then, the estimated flux expressed in (2.19) becomes:

$$\vec{\lambda}_{qdr}^s = \vec{\mu}\, T_c\, \vec{E}_c^s + \vec{\mu}\, \vec{\lambda}_{qdr}^{s^*} \tag{2.29}$$

The torque current i_{qs}^e in the synchronous reference frame is estimated from the stationary flux components by:

$$i_{qs}^e = \frac{i_{qs}^s \lambda_{dr}^s - i_{ds}^s \lambda_{qr}^s}{\sqrt{(\lambda_{dr}^s)^2 + (\lambda_{qr}^s)^2}} \tag{2.30}$$

2.2.3 Speed Estimation Scheme

The slip speed and synchronous speed can be calculated from the estimated rotor flux. It follows that the estimated rotor speed is the difference between the synchronous and slip speeds. The slip speed $s\,\omega_e$ in a rotor flux oriented drive is *uniquely* determined by the torque current i_{qs}^e and rotor flux magnitude $|\lambda_{dr}^e|$,

$$s\,\omega_e = \frac{R_r\, i_{qs}^e}{|\lambda_{dr}^e|} \tag{2.31}$$

with i_{qs}^e obtained from Equation (2.30), and the magnitude of the rotor flux obtained through:

$$|\lambda_{dr}^e| = \sqrt{(\lambda_{dr}^s)^2 + (\lambda_{qr}^s)^2} \tag{2.32}$$

The synchronous speed is also estimated from the rotor flux:

$$\omega_e = \frac{d\theta_e}{dt} \quad \text{and} \quad \theta_e = tan^{-1}(\frac{\lambda^s_{qr}}{\lambda^s_{dr}}) \tag{2.33}$$

$$\omega_e = \frac{\lambda^{s}_{qr}\lambda^s_{dr} - \lambda^s_{qr}\lambda^{s}_{dr}}{(\lambda^s_{dr})^2 + (\lambda^s_{qr})^2} \tag{2.34}$$

The rotor speed, therefore, is

$$\omega_{rm} = \omega_e - s\,\omega_e \tag{2.35}$$

2.2.4 Parameter Sensitivity and Low Speed Effects

In order to investigate the parameter sensitivity and low speed effects of the proposed estimation scheme, Equations (2.26) and (2.29) are combined to form:

$$\vec{\lambda}^s_{qdr} = \vec{\mu}\,T_c(\vec{E}^s_{qdr} + (\Delta R_s + j\omega_e\Delta L_\sigma)\,\vec{I}^s_{qds}) + \vec{\mu}\,\vec{\lambda}^{s^*}_{qdr} \tag{2.36}$$

Let

$$\vec{\lambda}^s_{qdr} = \vec{\lambda}_1 + \vec{\lambda}_2 + \vec{\lambda}_3 \tag{2.37}$$

Then

$$\vec{\lambda}_1 = \vec{\mu}\,T_c\,\vec{E}^s_{qdr} \tag{2.38}$$

$$\vec{\lambda}_2 = \vec{\mu}\,T_c\,(\Delta R_s + j\omega_e\Delta L_\sigma)\,\vec{I}^s_{qds} \tag{2.39}$$

$$\vec{\lambda}_3 = \vec{\mu}\,\vec{\lambda}^{s^*}_{qdr} \tag{2.40}$$

Parameter Sensitivity

It is observed that only $\vec{\lambda}_2$ is subjected to parameter variations, and thus the robustness of the estimator will improve if $\vec{\lambda}_2$ is negligibly small. The vector $\vec{\lambda}_2$ can be made to approximate zero by a proper selection of T_c, the filter time constant. To examine this, Equation (2.39) is re-written as:

$$\vec{\lambda}_2 = \vec{\mu}\,T_c\,\Delta Z\,\angle\gamma\,\vec{I}^s_{qds} \tag{2.41}$$

where

$$\Delta Z = \sqrt{\Delta R_s{}^2 + (\omega_e\Delta L_\sigma)^2} \tag{2.42}$$

and

$$\gamma = tan^{-1}(\frac{\omega_e\Delta L_\sigma}{\Delta R_s}) \tag{2.43}$$

Equation (2.41) can also be expressed as:

$$\vec{\lambda}_2 = T_c|\vec{\mu}|\Delta Z\angle(\phi+\gamma)\vec{I}^s_{qds} \tag{2.44}$$

Setting $\phi + \gamma = 0$,

$$tan^{-1}(\omega_e T_c) = tan^{-1}(\frac{\omega_e \Delta L_\sigma}{\Delta R_s}) \tag{2.45}$$

This requires that

$$T_c = \frac{\Delta L_\sigma}{\Delta R_s} \tag{2.46}$$

Note that

$$\frac{\Delta L_\sigma}{\Delta R_s} \doteq \frac{M}{R_r} \tag{2.47}$$

Thus, by choosing

$$T_c = \frac{M}{R_r} \tag{2.48}$$

which is exactly the rotor time constant, the phase of $\vec{\lambda}_2$ will be approximately zero. Likewise,

$$\Delta Z|\vec{\mu}| = 1 \tag{2.49}$$

Equation (2.44) can be written as:

$$\vec{\lambda}_2 = T_c \vec{I}^s_{qds} \tag{2.50}$$

As indicated, parameter sensitivity is minimized by minimizing $\vec{\lambda}_2$ in terms of both magnitude and phase angle.

Low Speed Effects

The performance improvement of the flux estimator is explained by examining $\vec{\lambda}_1$ and $\vec{\lambda}_3$ only, since $\vec{\lambda}_2$ is negligibly small. In a low speed range, $\vec{\lambda}_1$ will not be orthogonal to the back emf. The vector $\vec{\lambda}_3$ drives the vector $\vec{\lambda}_1$ to the correct position. Re-writing Equation (2.40) as:

$$\vec{\lambda}_3 = \frac{1}{\omega_e(\sqrt{1 + (\omega_e T_c)^2})} \angle(\phi - 90^o)\vec{E}^{s*}_{qdr} \tag{2.51}$$

and letting

$$\vec{E}^s_{qdr} = \vec{E}^{s*}_{qdr} \tag{2.52}$$

$\vec{\lambda}^s_{qdr}$ can be written:

$$\vec{\lambda}^s_{qdr} = |\vec{\mu}|\left(T_c \angle\phi + \frac{1}{\omega_e}\angle(\phi - 90^o)\right)\vec{E}^s_{qdr} \tag{2.53}$$

Examining Equation (2.53), $\vec{\lambda}_3$ adds the necessary amount of phase to make the back emf and flux orthongonal in a low speed range, and thus is the *compensating* component of the flux estimator.

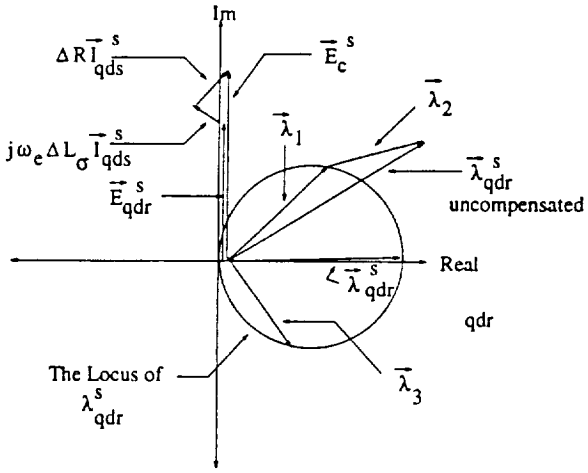

Figure 2.4: Phasor Diagram of Flux Estimator

A phasor diagram was constructed in Figure 2.4 to graphically illustrate how the components of the flux estimator are related. At low speeds, $\vec{\lambda}_1$ is not sufficiently shifted to be orthongonal to $\vec{E}^s_c$, such that the addition of $\vec{\lambda}_3$ will bring $\vec{\lambda}_1$ to its correct position. Also, as λ_2 approaches to zero, the sum of $\vec{\lambda}_2$ and $\vec{\lambda}_1$ approaches $\vec{\lambda}_1$, and the phase error due to the resistive parameters is reduced to a low level. Conversely, at high speeds $\vec{\lambda}_1$ is orthogonal to $\vec{E}^s_{qdr}$ and the magnitude of $\vec{\lambda}_3$ is quite small. In essence, the phase contribution of $\vec{\lambda}_3$ to $\vec{\lambda}_1$ is naturally reduced in a high speed range due to the low pass filter.

2.3 Computer Simulation and Laboratory Results

A computer simulation was conducted of the indirect field oriented system shown in Figure 2.5 to evaluate the performance of the estimator. The machine simulated has specifications listed in Table 1.

A triangular speed command is given ranging from +900 to -900 rpm. The stator resistance was varied 20 percent over 2 seconds. The phase current i_a and electromagnetic torque T_e are shown in Figure 2.6, while the actual and estimated rotor speed are shown in Figure 2.7.

The estimated speed follows the real speed, even in a low speed range, and is robust to the change in stator resistance.

Based on the excellent performance of the estimator, a position sensorless direct field oriented system was simulated as shown in Figure 2.8.

A triangular speed command was again given ranging from +900 rpm to -900 rpm. The phase current i_a and electromagnetic torque T_e are shown in Figure 2.9, while the rotor speed command and actual speed are shown in Figure 2.10.

The real speed follows the command speed, as the estimator peforms quite well over a wide speed range.

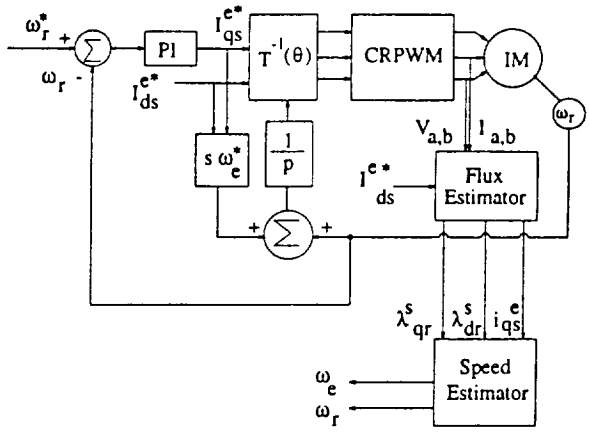

Figure 2.5: Indirect Field Oriented System with Position Sensor

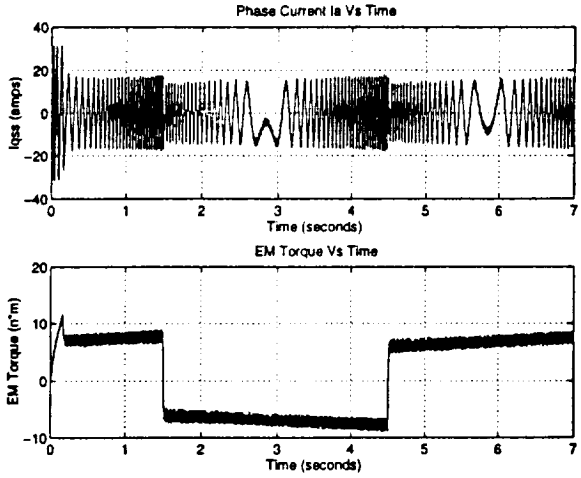

Figure 2.6: Phase Current and EM Torque

Table1

220 Volts	15 Amps	5 HP
$L_\sigma = 4$ mH	$M = 35.2$ mH	1800 rpm
$R_s = 1.1\,\Omega$	$R_r = .2696\,\Omega$	4 poles

2.4 Chapter Summary

A physical approach is presented for a position sensorless, field orientation controlled induction machine drive system. The key issue in a position sensorless drive is to observe the rotor flux correctly. Then the rotor speed can be calculated accurately.

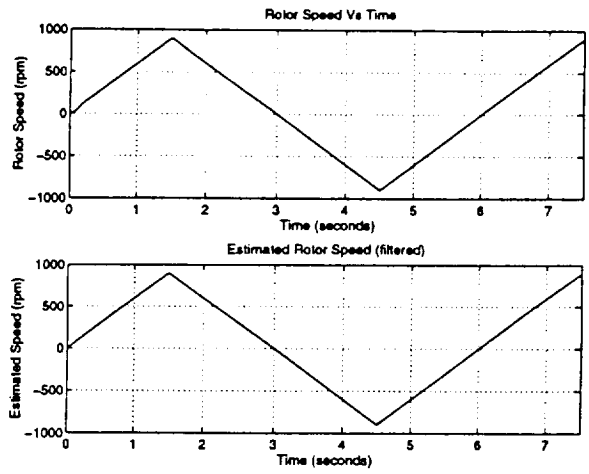

Figure 2.7: Real and Estimated Rotor Speed

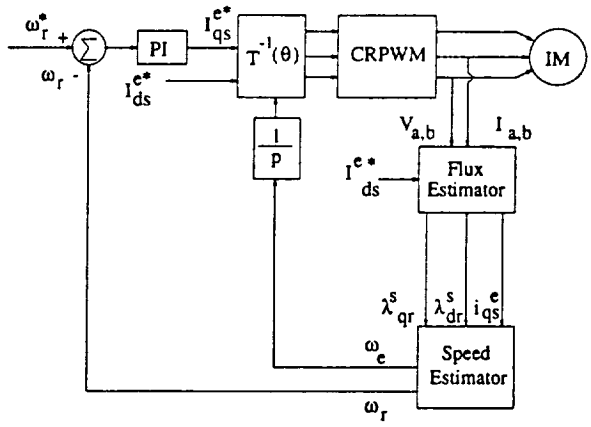

Figure 2.8: Position Sensorless Direct Field Oriented System

For the physical approach, the rotor flux is estimated accurately by making the rotor flux and back emf orthogonal even in a low speed range and subject to parameter variations. The algorithm simplicity is an attractive feature for implementation on a DSP real time control system.

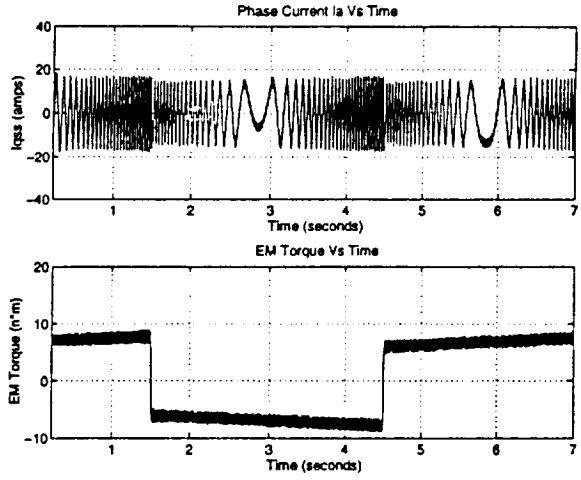

Figure 2.9: Phase Current and EM Torque

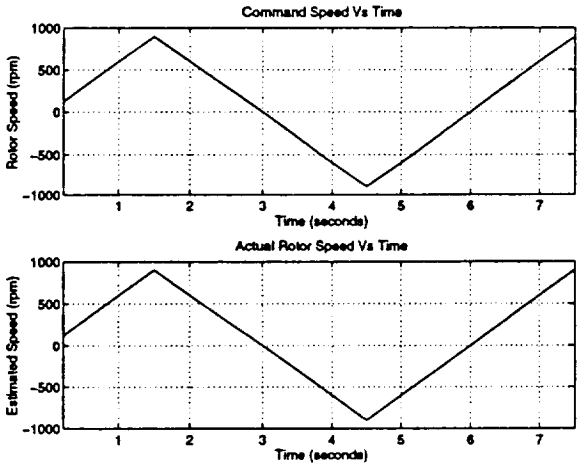

Figure 2.10: Command and Real Rotor Speed

3. Concluding Remarks

The general hardware and software organization of the DSP56001 develepment system has been discussed, and two application examples presented. The first application example is a field oriented BLDC machine, and the second example is a position sensorless induction machine drive.

The many noteworthy advantages of the DSP56KDSshould now be apparent. These advantages include a high clock speed and parallelism which allows for a high frequency sampling of feedback signals, thus the system is quite amenable to ac drive development.

Future work includes more thorough laboratory testing of the position sensorless induction machine drive discussed in this paper, as well as work in real time, on line estimation of machine parameters which are so critical for field oriented control. Here, the DSP56KDSwill be the major hardware component again. Additional future research will include case studies of specific systems which can employ position sensorless drives, including consideration of mechanical load charactersitics, the design of power converter and particular pwm scheme, etc.

4. References

[1] Y. Dote, "Servo Motor and Motion Control Using DSP",(book) Prentice-Hall

[2] C. J. Bonanno and L. Xu, "Robust, Parameter Insensitive Position Sensorless Field Orientation Control of the Induction Machine" *IEEE Power Electronics Specialist Conference,* Taipei, Taiwan, 1994.

[3] L. Xu and Y. Tang, "A Novel Wind-Power Generating System Using Field Orientation Controlled Doubly-Excited Brushless Reluctance Machine", *IEEE- IAS Annual Meeting,* Houston, Texas, 1992, pages 408-413.

[4] Y. Liao and Y. Tang, "A Low Cost, Robust Position Sensorless Control Scheme for Doubly-Fed Reluctance Motor Drives", *IEEE-IAS Annual Meeting,*1993, pages 437-444.

[5] H. Le-Huy and L. Dessaint, "An Adaptive Current Control Scheme for PWM Synchronous Motor Drives: Analysis and Simulation," *IEEE Transactions on Power Electronics,* volume 4, October 1989.

[6] S. Meshkat and E.K. Persson, "Optimum Current Vector Control of a Brushless Servo Amplifier Using Microprocessors," *IEEE-IAS Annual Meeting,* 1984, pages 451-457.

[7] T. Ohtani, N. Takada, and K. Tanaka, "Vector Control of Induction Motor Without Shaft Encoder," in *Proceedings of the IEEE-IAS Annual Conference,* 1989, pages 500-507.

[8] H.Tajima, Y. Hori, "Speed Sensorless Field-Orientation Control of the Induction Machine," *IEEE-IAS Transactions,* Vol. 29, No. 1, pages 175-180, January-February 1993.

[9] Kubota, H., Matsuse, K., and Nakano, T., "DSP-Based Speed Adaptive Flux Observer of Induction Motor," *IEEE-IAS Transactions,* Vol. 29,No. 2, pages 344-348, March-April 1993.

[10] X. Xu, R. De Doncker, and D. Novotny, "Implementation of Direct Stator Flux Orientation Control on a Versatile DSP Based System," *Proceedings of the IEEE-IAS Annual Conference,"* 1990, pages 404-409.

[11] X. Xu, and D. Novotny, "Selection of the Flux Reference for Induction Machine Drives in the Field Weakening Region," *IEEE-IAS Transactions,* Volume 28, No. 6, pages 1353-1358, November/December 1992.

[12] F.Z. Peng, and T. Fukao, "Robust Speed Identification for Speed Sensorless Vector Control of Induction Motors," *Proceedings of the IEEE-IAS Annual Conference,* 1993, pages 419-426.

[13] P.L. Jansen, R.D. Lorenz, and D.W. Novotny, "Observer-Based Field Orientation Analysis and Comparison of Alternative Methods," *Proceedings of the IEEE-IAS Annual Conference,* 1993, pages 536-543.

[14] C. Ferreira, S. Jones, W. Heglund, W. Jones, "Detailed Design of a 30-kW Switched Reluctance Starter/Generator System for a Gas Turbine Application," *1994 IEEE-IAS Conference Proceedings,* pages 97-105.

[15] U.S. Deshpande, J.J. Cathey, E. Richter, "A High Force Density Linear Switched Reluctance Machine," *1994 IEEE-IAS Conference Proceedings,* pages 251-257.

[16] B.K. Bose, T.J.E. Miller, P.M. Szczesny, and W.H. Bicknell, "Microcomputer Control of Switched Reluctance Motor," *IEEE-IAS Transactionss,* volume 22, number 4, July/August 1986, pages 708-715.